Received: 15 August 2018 | Accepted: 14 May 2019
DOI: 10.1002/hyp.13487

RESEARCH ARTICLE

WILEY

Measured and modelled above- and below-canopy turbulent fluxes for a snow-dominated mountain forest using GEOtop

Andrew T. Fullhart[1,2] | Thijs J. Kelleners[2] | Heather N. Speckman[3] | Daniel Beverly[3] | Brent E. Ewers[3] | John M. Frank[4] | William J. Massman[4]

[1] Hydrology Program, University of Wyoming, Laramie, Wyoming, USA
[2] Department of Ecosystem Science and Management, University of Wyoming, Laramie, Wyoming, USA
[3] Department of Botany, University of Wyoming, Laramie, Wyoming, USA
[4] Rocky Mountain Research Station, U.S. Forest Service, Fort Collins, Colorado, USA

Correspondence
Thijs J. Kelleners, Department of Ecosystem Science and Management, University of Wyoming, Laramie, WY, USA.
Email: tkellene@uwyo.edu

Funding information
National Science Foundation, Grant/Award Number: EPS-1208909

Abstract

The prediction of snowmelt in mountainous forests strongly depends on the accurate description of sensible and latent heat turbulent fluxes. Uncertainty about the within-canopy wind conditions especially poses a challenge, with relatively few studies examining both above- and below-canopy turbulent fluxes. In this study, turbulent flux predictions from a state-of-the-art watershed model GEOtop were verified against eddy covariance data from one above-canopy tower and two below-canopy towers in a snow-dominated coniferous forest in south-eastern Wyoming. The model was applied in one-dimensional vertical mode using field-observed vegetation parameters and laboratory-measured soil water retention data. The model was calibrated by identifying optimum values for the canopy fraction and the within-canopy eddy decay coefficient using the brute-force method. Above-canopy sensible heat flux at the Glacier Lakes Ecosystem Experiments Site was predicted reasonably well (r^2 = .851). The prediction of above-canopy latent heat flux was weaker (r^2 = .426). For latent heat flux, errors in 30-min values offset each other when fluxes were aggregated over time, resulting in realistic mean diurnal trends. Below-canopy turbulent flux at two sites in the Libby Creek Experimental Watershed were predicted with variable success with r^2 = .031–.146 for sensible heat flux and r^2 = .445–.581 for latent heat flux. Modelled below-canopy sensible heat flux was too low due to the underestimation of daytime ground surface temperature, because of not enough solar radiation reaching the soil surface. This study suggests that future work on GEOtop and related models should include better parameterizations of the ground surface energy balance to more reliably predict snowmelt and streamflow from mountainous forests.

KEYWORDS

forest, modelling, snow cover, surface energy balance

1 | INTRODUCTION

Streamflow from snow-dominated mountainous ecosystems is an important source of water in many parts of the world, including the Western United States (Bales et al., 2006). The timing of snowmelt is strongly influenced by the canopy and ground surface energy balances. These energy balances show high spatio-temporal variability with differences in elevation, slope, aspect, and vegetation cover, and diurnal and seasonal fluctuations in solar radiation, temperature, and precipitation, all playing a role. As a result, watershed computer simulation models for the complex mountain systems incorporate many bio-physical processes that are calculated at fine spatial and temporal resolutions (e.g., Endrizzi, Gruber, Dall Amico, & Rigon, 2014).

Turbulent exchange of water and heat between the ground surface, canopy, canopy air, and atmosphere plays an important part in the canopy and surface energy balance calculations. In forest, during daytime, sensible and latent heat fluxes are generally directed upwards from the ground to the atmosphere (Monson & Baldocchi, 2014), providing an important cooling mechanism against the incoming solar radiation. At night, sensible and latent heat fluxes generally have a much lower magnitude, and the flux direction may vary depending on the wind, temperature, and humidity conditions (Moene & van Dam, 2014). When the soil is snow covered (maximum ground surface temperature is 0°C and snow air water vapour pressure at saturation), the likelihood of downward sensible heat flux and upward latent heat flux increases.

Turbulent exchange between ecosystems and the atmosphere is generally described using the Monin–Obukhov similarity theory (Monin & Obukhov, 1954) that can be used to relate time-averaged vertical turbulent flux density to mean concentration gradients using the eddy diffusion coefficient. In the presence of thermal stratification, the eddy diffusion coefficient is modified using the Obukhov length (Monson & Baldocchi, 2014). Within the canopy, the shape of the wind and eddy diffusion profile have a significant impact on turbulent exchange. Most commonly, an exponential profile is assumed, resulting in relatively high wind and eddy diffusion near the top of the canopy (e.g., Dolman, 1993; Mahat, Tarboton, & Molotch, 2013).

Modelled turbulent fluxes are generally verified against eddy covariance data from above-canopy and/or below-canopy towers (e.g., Chen et al., 2014; Flerchinger, Reba, & Marks, 2012; Mahat et al., 2013). Such verification may be challenging given that eddy covariance measurements have their own limitations and sources of error. For example, eddy covariance measurements may be impacted by three-dimensional (3D) effects such as drainage and advection, by the inability to measure low-frequency contributions, and by stable atmospheric conditions at night (Massman & Lee, 2002). As a result, energy balance nonclosure is a common phenomenon that may be exacerbated by variable time lags in soil-plant energy storage, depending on the timescale used (Reed, Frank, Ewers, & Desai, 2017).

GEOtop is an open-source distributed watershed model suitable for simulating streamflow from snow-dominated mountainous regions (Endrizzi et al., 2014; Rigon, Bertoldi, & Over, 2006). The model uses Monin–Obukhov similarity theory and a within-canopy exponential wind/eddy diffusion profile to solve the canopy and ground surface energy balances at high spatial and temporal resolutions. GEOtop modelled turbulent fluxes have been verified previously against eddy covariance data from tundra sites (Endrizzi & Marsh, 2010), alpine grassland (Della Chiesa et al., 2014), and alpine foothills (Hingerl et al., 2016; Mauder et al., 2018).

In this study, GEOtop modelled turbulent fluxes are verified against eddy covariance data from snow-dominated mountainous coniferous forest. Above-canopy fluxes are verified by applying GEOtop in one-dimensional (1D) vertical mode to a 10-year record of above-canopy eddy covariance measurements at the Glacier Lakes Ecosystem Experiments Site (GLEES) in south-eastern Wyoming. In addition, below-canopy fluxes are verified by applying GEOtop to two sites with 3-year records of below-canopy eddy covariance measurements at the Libby Creek Experimental Watershed (LCEW), located about 3 km south-east of GLEES, at 200- to 250-m lower elevation. Taken together, the records from the three snow-dominated sites constitute a unique dataset with a level of detail that is rarely available for model verification (e.g., Mahat et al., 2013). The main goal of this study is to identify the strengths and weaknesses of GEOtop (and related models that employ similar physics) in calculating turbulent fluxes in a complex mountain environment. This is an important step towards more reliable snowmelt calculations in snow-dominated mountainous forest and improved streamflow predictions with GEOtop and similar physics-based watershed models.

2 | MODEL DESCRIPTION

GEOtop is an open-source physics-based distributed watershed model that calculates the canopy energy balance, the ground surface energy balance, canopy precipitation interception, multilayer snow, overland flow, 1D vertical snow-soil heat transport, 3D subsurface water flow, soil freeze–thaw, and channel flow (Endrizzi et al., 2014). The model accounts for the effect of elevation, slope, aspect, and vegetation cover on short wave and long wave radiation fluxes (Bertoldi et al., 2010) and is well suited for application in snow-dominated mountainous terrain. The model can be applied in 1D vertical mode (this study) and in distributed 3D mode (e.g., Fullhart, Kelleners, Chandler, McNamara, & Seyfried, in press).

2.1 | Above-canopy turbulent fluxes

The sensible heat flux between the canopy air and the above-canopy atmosphere H (J m^{-2} s^{-1}) equals the sum of the canopy to canopy air sensible heat flux H_v (J m^{-2} s^{-1}) and the ground surface to canopy air sensible heat flux H_g (J m^{-2} s^{-1}; i.e., $H = H_v + H_g$). Similarly, the latent heat flux between the canopy air and the above-canopy atmosphere LE (J m^{-2} s^{-1}) equals the sum of the canopy to canopy air latent heat flux LE_v (J m^{-2} s^{-1}) and the ground surface to canopy air latent heat flux LE_g (J m^{-2} s^{-1}; i.e., $LE = LE_v + LE_g$). Values for H and LE are calculated using the following (Endrizzi & Marsh, 2010):

$$H = \rho_a c_p \frac{T_{ca} - T_a}{r_{aH}}, \tag{1a}$$

$$LE = L\rho_a \frac{q_{ca} - q_a}{r_{aE}}, \tag{1b}$$

where ρ_a is air density (kg m^{-3}), c_p is specific heat capacity at constant pressure (J kg^{-1} K^{-1}), T_{ca} is canopy air temperature (°C), T_a is atmospheric air temperature (°C), r_{aH} is above-canopy aerodynamic resistance for heat transfer (s m^{-1}), L is latent heat of vaporization (J kg

$^{-1}$), q_{ca} is canopy air specific humidity (kg kg^{-1}), q_a is atmosphere specific humidity (kg kg^{-1}), and r_{aE} is above-canopy aerodynamic resistance for water vapour (s m^{-1}).

2.2 | Canopy energy balance

The canopy energy balance is given as follows (Endrizzi and marsh, 2010):

$$C_v \frac{dT_v}{dt} = SW_v + LW_v - H_v - LE_v, \tag{2}$$

where C_v is canopy height-integrated heat capacity (J m^{-2} K^{-1}), T_v is canopy temperature (°C or K), t is time (s), SW_v is absorbed short wave radiation (J m^{-2} s^{-1}), and LW_v is absorbed long wave radiation (J m^{-2} s^{-1}). Values for SW_v, LW_v, H_v, and LE_v are calculated as follows (Endrizzi & Marsh, 2010):

$$SW_v = \sum_{\Lambda} \left(SW_{atm}{\downarrow}^{\mu}_{\Lambda} \overrightarrow{I}^{\mu}_{\Lambda} + SW_{atm}{\downarrow}_{\Lambda} \overrightarrow{I}_{\Lambda} \right), \tag{3a}$$

$$\begin{aligned} LW_v = {} & \varepsilon_v [1 + (1 - \varepsilon_g)(1 - \varepsilon_v)] LW_{atm}{\downarrow} \\ & + \varepsilon_v \varepsilon_g \sigma T_g^4 - [2 - \varepsilon_v (1 - \varepsilon_g)] \varepsilon_v \sigma T_v^4, \end{aligned} \tag{3b}$$

$$H_v = \rho_a c_p \frac{T_v - T_{ca}}{r_b}, \tag{3c}$$

$$LE_v = L \rho_a \frac{q_v - q_{ca}}{r_c + r_b}, \tag{3d}$$

where $SW_{atm}{\downarrow}$ is incoming short wave radiation (J m^{-2} s^{-1}), $LW_{atm}{\downarrow}$ is incoming long wave radiation (J m^{-2} s^{-1}), $\overrightarrow{I}$ is absorbed solar radiation per unit incoming short wave radiation (—), ε_v is canopy emissivity (—), ε_g is ground emissivity (—), σ is Stefan–Boltzmann constant (5.67 × 10^{-8} J m^{-2} s^{-1} K^{-4}), T_g is ground surface temperature (°C or K), q_v is canopy specific humidity (kg kg^{-1}), r_c is stomatal resistance (s m^{-1}), and r_b is leaf boundary resistance (s m^{-1}). The subscript Λ denotes waveband (visible and near-infrared), and the superscript μ denotes direct beam radiation (as opposed to diffuse radiation). Note that Equation (3b) assumes that absorptivity equals emissivity.

2.3 | Ground surface energy balance

The ground surface is either soil or snow. The ground surface energy balance is as follows (Endrizzi et al., 2014):

$$SW_g + LW_g = H_g + LE_g + G, \tag{4}$$

where SW_g is ground surface net short wave radiation (J m^{-2} s^{-1}), LW_g is ground surface net long wave radiation (J m^{-2} s^{-1}), and G is ground heat flux (J m^{-2} s^{-1}). Values for SW_g, LW_g, H_g, and LE_g are calculated as follows (Endrizzi & Marsh, 2010; Fullhart, Kelleners, Chandler, McNamara, & Seyfried, 2018):

$$\begin{aligned} SW_g = {} & \mathrm{CF} \sum_{\Lambda} \left[SW_{atm}{\downarrow}^{\mu}_{\Lambda} e^{-\kappa \mathrm{LAI}} \left(1 - \alpha^{\mu}_{g,\Lambda}\right) + \left(SW_{atm}{\downarrow}^{\mu}_{\Lambda} I{\downarrow}^{\mu}_{\Lambda} + SW_{atm}{\downarrow}_{\Lambda} I{\downarrow}_{\Lambda}\right)\left(1 - \alpha_{g,\Lambda}\right) \right] \\ & + (1 - \mathrm{CF}) \sum_{\Lambda} \left[SW_{atm}{\downarrow}^{\mu}_{\Lambda} \left(1 - \alpha^{\mu}_{g,\Lambda}\right) + SW_{atm}{\downarrow}_{\Lambda} \left(1 - \alpha_{g,\Lambda}\right) \right], \end{aligned} \tag{5a}$$

$$\begin{aligned} LW_g = {} & \mathrm{CF} \left(\varepsilon_g (1 - \varepsilon_v) LW_{atm}{\downarrow} + \varepsilon_g \varepsilon_v \sigma T_v^4 - \varepsilon_g \sigma T_g^4 \right) \\ & + (1 - \mathrm{CF}) \left(\varepsilon_g LW_{atm}{\downarrow} - \varepsilon_g \sigma T_g^4 \right), \end{aligned} \tag{5b}$$

$$H_g = \mathrm{CF} \rho_a c_p \frac{T_g - T_{ca}}{r_{uc}} + (1 - \mathrm{CF}) \rho_a c_p \frac{T_g - T_a}{r_{aH}}, \tag{5c}$$

$$LE_g = \mathrm{CF} L \rho_a \beta \frac{\alpha q_g^{sat} - q_{ca}}{r_{uc}} + (1 - \mathrm{CF}) L \rho_a \beta \frac{\alpha q_g^{sat} - q_a}{r_{aE}}, \tag{5d}$$

where CF is canopy fraction (—), LAI is leaf area index (m^2 m^{-2}), κ is decay coefficient (—), α_g is ground albedo (—), I is diffuse flux per unit incoming direct beam and diffuse short wave radiation (—), r_{uc} is undercanopy resistance to sensible and latent heat fluxes (s m^{-1}), q_g^{sat} is ground surface saturated specific humidity (kg kg^{-1}); and the dimensionless reduction factors α and β are determined by the Kelvin equation and the Lee and Pielke (1992) empirical equation, respectively. Note that the equations used for α and β differ from those of Ye and Pielke (1993) as used in the original GEOtop model. For details, see Fullhart et al. (2018).

2.4 | Turbulent flux resistance factors

The above-canopy aerodynamic resistance factors are calculated using the Monin–Obukhov similarity theory (e.g., Moene & van Dam, 2014):

$$r_{aH} = \frac{1}{k^2 v_a} \left[\ln\left(\frac{z_a - d}{z_{0m}}\right) - \Psi_m\left(\frac{z_a - d}{L}\right) + \Psi_m\left(\frac{z_{0m}}{L}\right) \right] \left[\ln\left(\frac{z_a - d}{z_{0H}}\right) - \Psi_H\left(\frac{z_a - d}{L}\right) + \Psi_H\left(\frac{z_{0H}}{L}\right) \right], \tag{6a}$$

$$r_{aE} = \frac{1}{k^2 v_a} \left[\ln\left(\frac{z_a - d}{z_{0m}}\right) - \Psi_m\left(\frac{z_a - d}{L}\right) + \Psi_m\left(\frac{z_{0m}}{L}\right) \right] \left[\ln\left(\frac{z_a - d}{z_{0E}}\right) - \Psi_E\left(\frac{z_a - d}{L}\right) + \Psi_E\left(\frac{z_{0E}}{L}\right) \right], \tag{6b}$$

where k is dimensionless von Karman constant; v_a is measured above-canopy wind speed (m s^{-1}); z_a above-canopy measurement height (m); d is zero-plane displacement height (m); $\Psi_m(\zeta)$, $\Psi_H(\zeta)$, and $\Psi_E(\zeta)$ are dimensionless functions; L is Obukhov length (m); and z_{0m}, z_{0H}, and z_{0E} (m) are vegetation roughness lengths for momentum, sensible heat, and latent heat, respectively. The stomatal resistance is given by the following (Best, 1998; Rigon et al., 2006):

$$r_c = \frac{r_{c,\min}}{\mathrm{LAI}(f_S f_e f_T f_w)}, \tag{7}$$

where $r_{c,min}$ is minimum stomatal resistance (s m^{-1}); and f_S, f_e, f_T, and f_w are dimensionless functions describing the impact of solar radiation, water vapour pressure deficit, temperature, and soil moisture, respectively. The leaf boundary resistance in GEOtop was updated by Fullhart et al. (2018) assuming an exponential within-canopy wind profile and reads as follows (Mahat et al., 2013):

$$r_b = 100 n_e \sqrt{d_{leaf}/v_{zveg}} / 2[1 - \exp(-n_e/2)]\mathrm{LAI}, \quad (8)$$

where n_e is dimensionless eddy decay coefficient, d_{leaf} is characteristic dimension of the leaves in the wind flow direction (m), and v_{zveg} is wind speed at the vegetation height (m s^{-1}). The proportionality factor of 100 has units of $s^{0.5}$ m^{-1}. The undercanopy resistance (exponential within-canopy wind profile) is given by the following (Endrizzi & Marsh, 2010):

$$r_{uc} = \frac{z_{veg}}{n_e D_{e,zveg}} \left\{ \exp\left[n_e\left(1 - \frac{z_{0g}}{z_{veg}}\right)\right] - \exp\left[n_e\left(1 - \frac{d + z_{0v}}{z_{veg}}\right)\right]\right\}, \quad (9)$$

where z_{veg} is vegetation height (m), $D_{e,zveg}$ is eddy diffusion coefficient (m^2 s^{-1}) at z_{veg}, and z_{0g} and $z_{0v} = z_{0m}$ (m) are the ground and vegetation roughness lengths, respectively. For canopy fractions < 1 (=partial ground cover), GEOtop uses Equation (6) for the bare ground fraction, with d = 0 and z_{0m}, z_{0H}, and z_{0E} representing ground roughness lengths. Under these conditions, below-canopy turbulent fluxes are calculated by taking the weighted average from the vegetated and bare ground fractions while continuing to solve for a single ground surface temperature at each time step.

2.5 | Soil hydraulic properties

The soil hydraulic properties are described using the Mualem (1976) and van Genuchten (1980) equations:

$$K = K_s S_e^{\lambda}\left[1 - \left(1 - S_e^{1/m}\right)^m\right]^2 \times 10^{-\omega\Omega}, \quad (10)$$

$$S_e = \frac{\theta_w - \theta_r}{\theta_s - \theta_r} = \frac{1}{\left[1 + (-\alpha_{vg} h)^n\right]^m} \;\; h < 0, \quad (11)$$

where K is hydraulic conductivity (m s^{-1}); K_s saturated hydraulic conductivity (m s^{-1}); S_e dimensionless relative saturation; λ dimensionless tortuosity parameter; n dimensionless pore size distribution parameter, $m = 1 - 1/n$; ω dimensionless coefficient; Ω fractional ice content; θ_w soil water content (m^3 m^{-3}); θ_r residual soil water content (m^3 m^{-3}); θ_s saturated soil water content (m^3 m^{-3}); h soil water pressure head (m); and α_{vg} inverse of the air entry soil water pressure head (m^{-1}).

2.6 | Model statistics

The quality of the GEOtop model predictions is evaluated using the coefficient of determination (r^2), the root mean square error (RMSE), the modelling efficiency (ME), and the coefficient of residual mass (CRM; e.g., Loague & Green, 1991):

$$r^2 = 1 - \frac{\sum_{i=1}^{n}(O_i - P_i)^2}{\sum_{i=1}^{n}(O_i - \overline{O})^2}, \quad (12)$$

$$\mathrm{RMSE} = \left[\frac{1}{n}\sum_{i=1}^{n}(P_i - O_i)^2\right]^{0.5}, \quad (13)$$

$$\mathrm{ME} = \frac{\sum_{i=1}^{n}(O_i - \overline{O})^2 - \sum_{i=1}^{n}(P_i - O_i)^2}{\sum_{i=1}^{n}(O_i - \overline{O})^2}, \quad (14)$$

$$\mathrm{CRM} = \frac{\sum_{i=1}^{n} O_i - \sum_{i=1}^{n} P_i}{\sum_{i=1}^{n} O_i}, \quad (15)$$

where n is the number of samples, P_i the predicted values, and O_i the observed data.

3 | ABOVE-CANOPY TURBULENT FLUXES: GLEES

GEOtop modelled turbulent fluxes were verified against data from an above-canopy eddy covariance tower at the GLEES in south-eastern Wyoming. GLEES is located on the eastern slope of the Medicine Bow Mountains about 75 km west of Laramie, WY. The eddy covariance tower is located in a mixed Engelmann spruce and subalpine fir forest at 3,197 m above mean sea level. This tower is considered one of the windiest eddy covariance sites in North America (Speckman et al., 2015). The climate is subalpine continental (Dfc) according to the Köppen classification. The annual water balance is snow dominated with mean annual air temperature of 0.1°C and mean annual precipitation of 1,330 mm. The area is generally snow covered from November to June. The topography of GLEES is complex owing to the mountainous setting, with the area around the eddy covariance tower being relatively flat.

A 10-year simulation period was selected from August 1, 2005, to July 31, 2015. Starting the simulation on August 1 has the benefit of relatively well-defined initial conditions as soils will be relatively dry and warm and without snow cover. Climate data (30-min interval) to drive the GEOtop model (precipitation, wind speed, wind direction, relative humidity, air temperature, incoming solar radiation, and incoming long wave radiation) were downloaded from the AmeriFlux website (http://ameriflux.lbl.gov). Data to verify the GEOtop model simulation (outgoing short wave radiation, outgoing long wave radiation, sensible heat flux, latent heat flux, ground heat flux, and soil temperature) were obtained from the same source. Above-canopy sensors were 22.6 to 25.8 m above the soil surface, with the forest canopy reaching to about 18 m. Ground heat flux was measured at 9 cm below the soil surface, while soil temperature was measured at 10-cm depth. A detailed description of the instrumentation at the GLEES eddy covariance tower is given in Frank, Massman, Ewers, Huckaby, and Negrón (2014) and is not repeated here. Additional data to verify the GEOtop modelled snowpack (snow depth and snow water equivalent at 1 to 4-hr intervals) were obtained from the Brooklyn Lake SNOTEL site (https://wcc/sc/egov.usda.gov/nwcc) that is ~0.5 km to the south-east of the eddy covariance tower with roughly the same elevation and forest structure.

A 2-m-deep soil profile was assumed in the model with three layers. Soil samples were obtained from a 0.5-m-deep soil pit dug

~50 m to the south of the eddy covariance tower. The soil at the site is heterogeneous with a high stone content, making it impossible to obtain representative undisturbed samples for dry bulk density determination. Grab samples were air dried in the laboratory, crushed, and sieved to <2-mm diameter. Soil texture for the three layers was determined using the hydrometer method (Table 1). Gravimetric soil water retention for the three layers was measured in the laboratory using a WP4 dew-point potentiometer (Decagon Devices, Pullman, WA), a pressure plate apparatus (Dane & Hopmans, 2002a), and hanging water columns (Dane & Hopmans, 2002b). The gravimetric water retention data were converted to volumetric water retention data using estimated dry bulk density values ρ_b (defined here as $M_{<2mm}/V_T$) for each layer, where $M_{<2mm}$ is the mass of soil particles < 2 mm in diameter and V_T is the total volume (Russo, 1983). The van Genuchten (1980) water retention parameters were obtained by curve fitting the volumetric water retention data. Saturated hydraulic conductivity for the three layers was estimated using the Kozeny–Carman equation (Bear, 1972). It was assumed that coarse fragments > 2 mm do not contribute to water retention or hydraulic conductivity. The resulting soil hydraulic parameters in the Mualem (1976) and van Genuchten (1980) models for the three layers are given in Table 2. In GEOtop, it was assumed that the 0.5- to 2.0-m soil has the same hydraulic properties as the 25- to 50-cm layer.

Vegetation in GEOtop was described using vegetation height = 18 m, reference leaf area index LAI_{ref} = 3.0 m^2 m^{-2}, $r_{c,min}$ = 125 s m^{-1} (Equation 7), and rooting depth = 2.5 m. Canopy fraction CF was varied between 0 and 1 as part of the model calibration. Leaf area index was calculated as LAI = LAI_{ref}/CF. With CF < 1, the forest is described as an ensemble of trees and open spaces with separate wind functions. Leaf area index in this case is relatively high, approaching the LAI of individual trees. With CF = 1, the forest is described as a uniform ecosystem with a single wind function and relatively low LAI = LAI_{ref}. The dimensionless eddy decay coefficient n_e was also varied as part of the model calibration. Reported values for n_e usually vary between 0.4 and 4.0 (Brutsaert, 1982; Kochendorfer & Ramirez, 2010), although values as high as 6.0 have been used for coniferous forest (Kelleners et al., 2016). Canopy fraction (0 to 1) and n_e (1 to 10) were varied simultaneously using the brute-force method with the objective function consisting of both the sensible and latent heat fluxes. In the objective function, the sum of squared errors between measured and modelled values was weighted by the number of data points and the measurement variances to give equal weight to both types of turbulent fluxes (e.g., Clausnitzer & Hopmans, 1995).

There is some uncertainty associated with the vegetation parameters because of a spruce beetle outbreak that became epidemic in 2008, resulting in significant tree mortality at GLEES (Frank et al., 2014). As a first approximation, vegetation parameters were kept constant with time in this study with a relatively low value of LAI_{ref} = 3.0 m^2 m^{-2} to reflect the tree mortality. GEOtop was initialized by running the model twice, where the first 10-year simulation period served as a warm-up period for the second 10-year simulation period to ensure realistic initial water contents and temperatures for the 2-m soil profile. The top boundary condition was determined by incoming precipitation and the canopy and ground surface energy balances (Equations 2 and 4). The bottom boundary condition for soil water flow was zero pressure head gradient (=free drainage). The bottom boundary condition for soil heat transport was zero temperature gradient.

A contour plot of the objective function values for all tested combinations of canopy fraction CF and the eddy decay coefficient n_e is shown in Figure 1c. For comparison, the results with only weighted sensible heat flux (Figure 1a) and only weighted latent heat flux (Figure 1b) in the objective function are also shown. The value of the objective function is presented as a dimensionless root mean square error $RMSE_w$ value owing to the weighting procedure used. The best results (lowest $RMSE_w$ value) were obtained for CF = 0.7 and n_e = 6.5 (Figure 1c). The contour plots suggest that combinations with CF $\geq$ 0.7 and n_e > 6 produce relatively similar model error (Figure 1a–c), indicating that there is considerable uncertainty in the "true" CF and n_e values. With the use of LAI = LAI_{ref}/CF, the resulting optimum leaf area index LAI = 3.0/0.7 = 4.3.

Measured and GEOtop modelled above-canopy net radiation, sensible heat flux, and latent heat flux are shown in Figure 2, together with below-canopy snow depth, snow water equivalent, ground heat flux, and soil temperature. The 30-min to 4-hr measured values and the 30-min modelled values are averaged to daily, weekly, or monthly values to facilitate visual comparison for the entire 10-year period. Net radiation (positive downwards) is the sum of net short wave radiation and net long wave radiation. Sensible heat flux and latent heat flux are defined as positive upwards, whereas ground heat flux is defined as positive downwards. Additional model statistics are summarized in Table 3.

TABLE 1 Soil texture data (hydrometer method) for the eddy covariance tower at the Glacier Lakes Ecosystem Experiments Site on the eastern slope of the Medicine Bow Mountains in south-eastern Wyoming

Depth (cm)	Sand (%)	Silt (%)	Clay (%)	Class
0–6	33	55	12	Silt loam
6–25	41	45	14	Loam
25–50	45	50	5	Sandy loam

TABLE 2 Estimated soil dry bulk density ρ_b, optimized residual soil water content θ_r, optimized saturated soil water content θ_s, optimized inverse of the air entry soil water pressure head α_{vg}, optimized pore size distribution parameter n, and calculated saturated soil hydraulic conductivity K_s for the eddy covariance tower at the Glacier Lakes Ecosystem Experiments Site on the eastern slope of the Medicine Bow Mountains in south-eastern Wyoming

Depth (cm)	ρ_b (g cm^{-3})	θ_r (cm^3 cm^{-3})	θ_s (cm^3 cm^{-3})	α_{vg} (cm^{-1})	n	K_s (cm d^{-1})
0–6	0.7	0.000	0.661	0.020	1.270	291
6–25	1.2	0.000	0.535	0.012	1.294	122
25–200	1.3	0.012	0.448	0.006	1.469	170

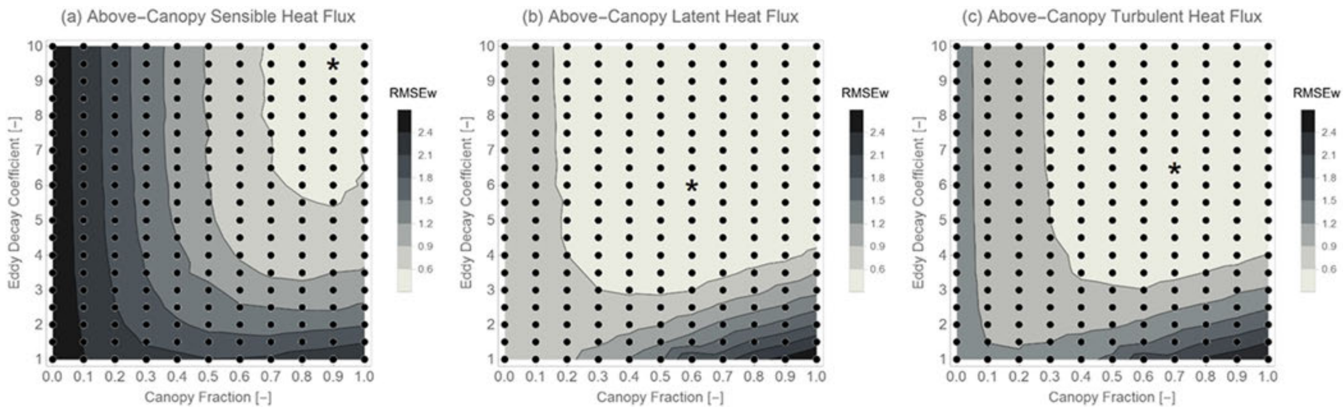

FIGURE 1 Contour plots of model error (expressed as dimensionless weighted root mean square error $RMSE_w$) as a function of canopy fraction and within-canopy eddy decay coefficient for the above-canopy eddy covariance tower at the Glacier Lakes Ecosystem Experiments Site in south-eastern Wyoming. The dots represent individual model runs. The stars represent the parameter combinations with the lowest model error. Model error was calculated using a weighted objective function containing 30-min above-canopy sensible heat flux (a), latent heat flux (b), and sensible and latent heat fluxes combined (c)

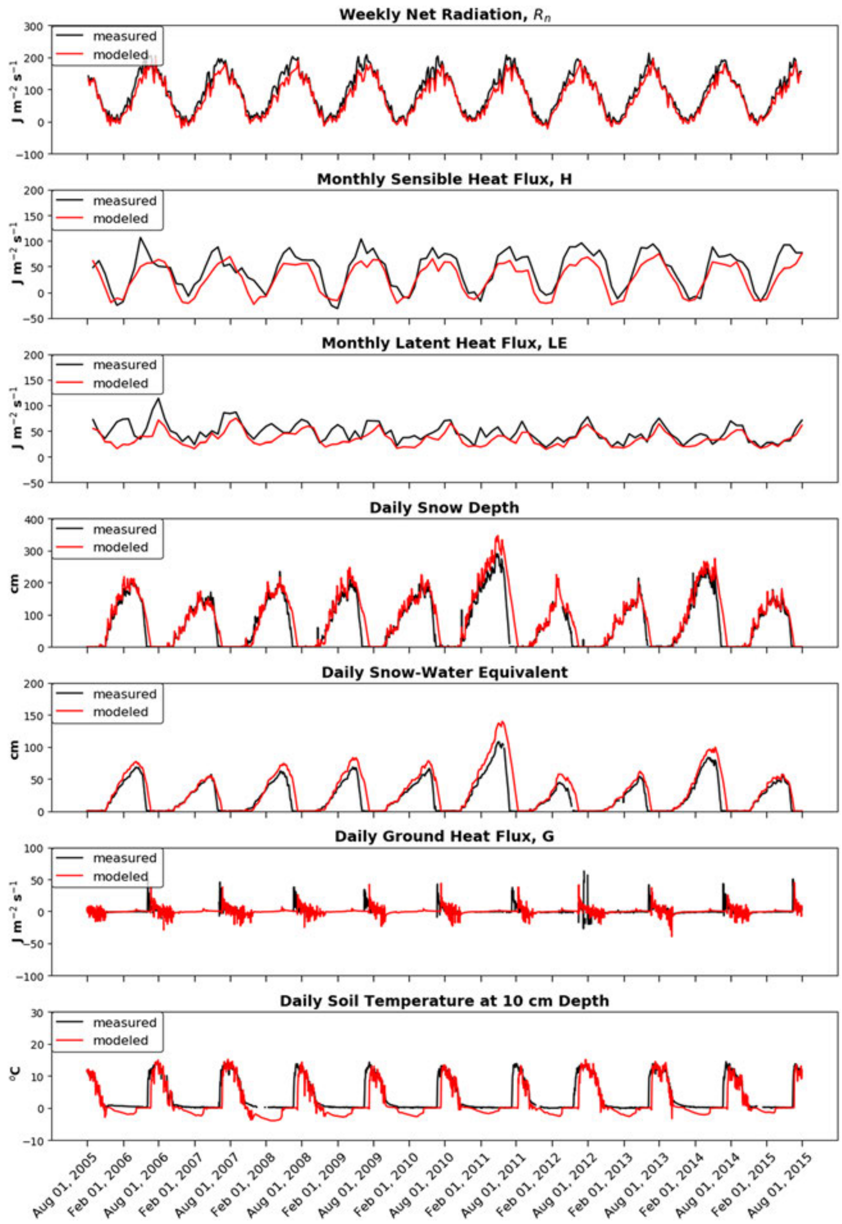

FIGURE 2 Measured and GEOtop modelled above-canopy net radiation, above-canopy sensible heat flux, above-canopy latent heat flux, snow depth, snow water equivalent, ground heat flux, and soil temperature (10-cm depth) for August 2005 to July 2015 for the above-canopy eddy covariance tower at the Glacier Lakes Ecosystem Experiments Site in south-eastern Wyoming

TABLE 3 Calculated 30-min to 4-hr interval RMSE, ME, and CRM for the GEOtop model application for the eddy covariance tower at the Glacier Lakes Ecosystem Experiments Site on the eastern slope of the Medicine Bow Mountains in south-eastern Wyoming

Model component	RMSE	ME	CRM
Above-canopy net radiation	77.35 J m^{-2} s^{-1}	0.90	0.15
Above-canopy sensible heat flux	62.35 J m^{-2} s^{-1}	0.84	0.34
Above-canopy latent heat flux	45.63 J m^{-2} s^{-1}	0.33	0.26
Snow depth	29.26 cm	0.85	−0.15
Snow water equivalent	15.26 cm	0.63	−0.33
Ground heat flux	30.07 J m^{-2} s^{-1}	−0.12	0.43
Soil temperature at 10-cm depth	3.34°C	0.55	0.45

Abbreviations: CRM, coefficient of residual mass; ME, modelling efficiency; RMSE, root mean square error.

Figure 2 shows that most of the net radiation in the summer is partitioned into sensible heat flux with the latent heat flux being roughly half the sensible heat flux in most summers. Figure 2 also shows that snow accumulation is captured well by the GEOtop model whereas snow melt-off is delayed. The delay in modelled snow melt-off results in delayed soil warm-up as shown in the ground heat flux and soil temperature panels. Modelled soil temperatures are too far below zero in winter. The low modelled winter soil temperatures occur at the start of the winter periods when the snowpack is still developing. Later in the snow season, the insulating properties of the fully developed snowpack and upward heat flux from the subsurface combine to bring the modelled soil temperatures back up to ~0°C.

Scatter plots comparing the 30-min with 4-hr measured and modelled values (not shown) have relatively high coefficient of determination for sensible heat flux (r^2 = .851) and lower coefficient of determination for latent heat flux (r^2 = .426) and ground heat flux (r^2 = .326). The above-canopy latent heat flux is the result of transpiration from root water uptake, evaporation of canopy-intercepted precipitation, and evaporation from the ground surface (either soil or snow). The first two years of the simulation period (August 2005 to July 2007), that is, before the spruce beetle outbreak, had about the same r^2 = .388 for *LE* as the following eight years (August 2007 to July 2015) with r^2 = .441. This suggests that the relatively low model performance for *LE* is unrelated to the spruce beetle outbreak. The relatively low coefficient of determination for ground heat flux is explained, at least in part, by the delayed snow melt-off as simulated by GEOtop.

Mean diurnal variations in above-canopy sensible and latent heat fluxes for different periods and conditions are shown in Figure 3. The figure shows that daytime *H* is generally underestimated by GEOtop, except in summer and during low wind conditions (<1 m s^{-1}). Figure 3 also shows that daytime *LE* values are considerably lower than daytime *H* values. The GEOtop model captures the diurnal variations in *LE* surprisingly well, in spite of the relatively low r^2 value for *LE*. This indicates that the modelled *LE* value for a certain time period may be significantly off but that the average dynamics in *LE* are captured well. The most significant discrepancies between measured and modelled *LE* occur in winter and under low wind conditions when daytime *LE* is underestimated by the model. Scatter plots with 30-min measured versus 30-min modelled values (not shown) exhibit night-time *H* and *LE* with relatively low r^2 values of.505 versus.215, respectively. This may be due to stable atmospheric conditions at night that reduce the eddy covariance instrument response (Massman & Lee, 2002).

4 | BELOW-CANOPY TURBULENT FLUXES: LCEW, SOUTH-FACING SLOPE

The GEOtop modelled turbulent fluxes were further verified against data from a below-canopy eddy covariance tower on a south-facing slope at the LCEW in south-eastern Wyoming. LCEW is located on the eastern slope of the Medicine Bow Mountains about 3 km south-east of GLEES. The eddy covariance tower is located in a mixed lodgepole pine, Engelmann spruce, and subalpine fir forest at 2,950 m above mean sea level. The annual water balance is snow dominated with estimated mean annual air temperature of 1.7°C and estimated mean annual precipitation of 1,160 mm. The slope (length = 75 m; aspect = 180°; angle = 22°) is generally snow covered from November to May (Pleasants, Kelleners, & Ohara, 2017).

A 3-year simulation period was selected from November 1, 2014, to October 31, 2017, dictated mostly by the availability of eddy covariance data. Climate data (30-min interval) to drive the GEOtop model were from the same source as before (the above-canopy eddy covariance tower at GLEES) and were adjusted for differences in elevation using lapse rates given in Liston and Elder (2006). Below-canopy sensible and latent heat fluxes (30-min interval) were determined using a Campbell Scientific IRGASON integrated open-path analyser and sonic anemometer installed at 3.5 m above the soil surface and measuring at 10 Hz. The 30-min average values of temperature, relative humidity, and atmospheric pressure from the IRGASON were used to calculate canopy air temperature and canopy air specific humidity. Snow depth (2-hr interval) was measured using a down-facing Campbell Scientific SR50 acoustic distance sensor. Ground surface temperature (2-hr interval) was measured using a down-facing Apogee SI-111 infrared radiometer. Soil temperature (2-hr interval) was measured using Stevens Hydra probes installed at 10, 30, and 50 cm below the soil surface.

A 1.5-m-deep soil profile was assumed in the model with four layers. Soil samples were obtained from a 1.0-m-deep soil pit near the eddy covariance tower. High stone content again prevented the collection of representative undisturbed samples. Instead, grab samples were collected and dried, crushed, and sieved (<2-mm diameter) in the laboratory. Soil texture for the four layers (Table 4) and soil hydraulic parameters (Table 5) were determined using similar methods as for the GLEES site discussed earlier. In GEOtop, it was assumed that the 1.0- to 1.5-m soil has the same hydraulic properties as the 50- to 100-cm layer.

The same vegetation parameters were selected in GEOtop as for GLEES. The optimum canopy fraction and eddy decay coefficient were

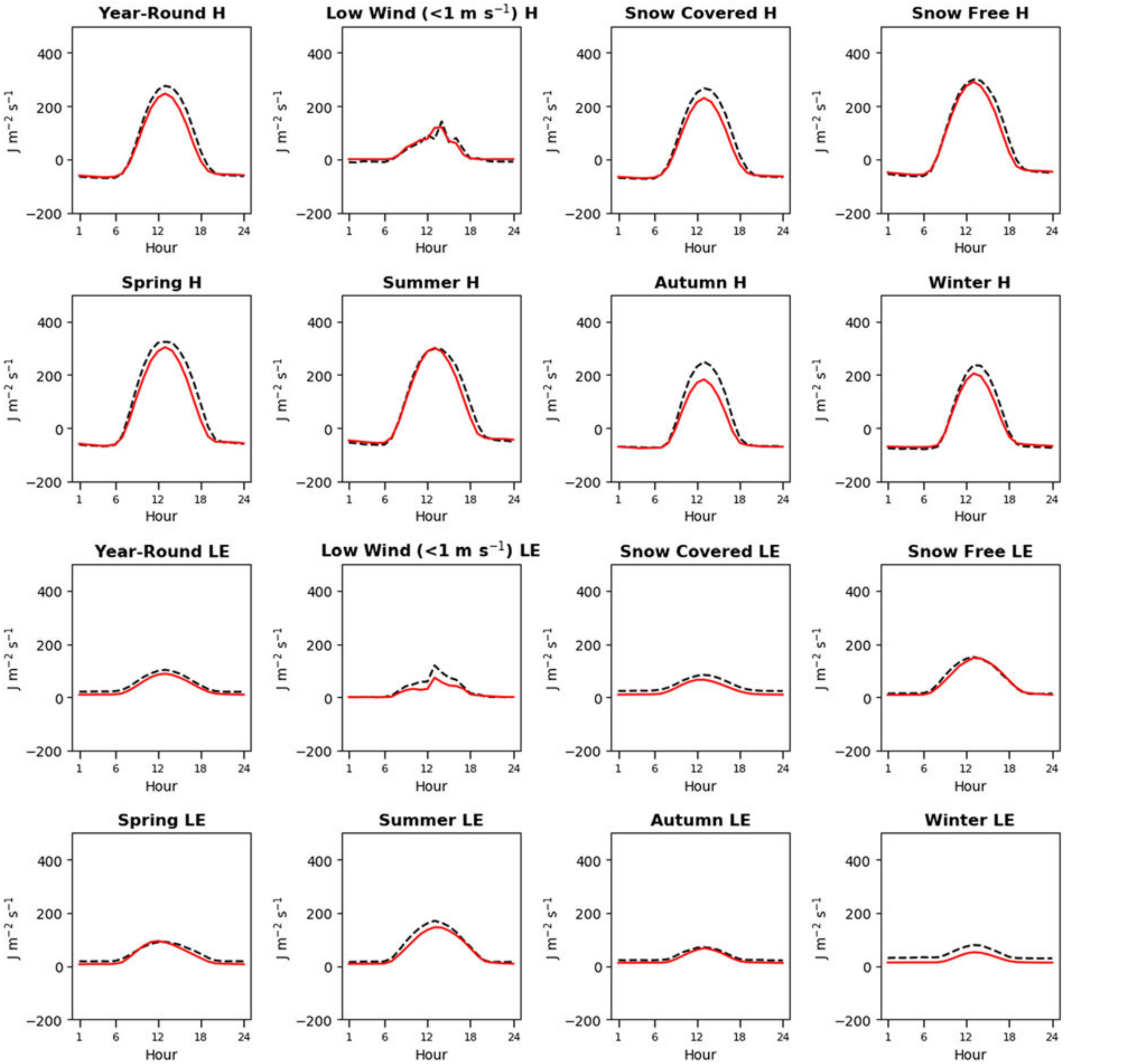

FIGURE 3 Mean diurnal variation of above-canopy sensible heat flux *H* and above-canopy latent heat flux *LE* for different periods and conditions during the August 2005 to July 2015 study period for the above-canopy eddy covariance tower at the Glacier Lakes Ecosystem Experiments Site in south-eastern Wyoming. Both measured (black dashed lines) and GEOtop modelled (red continuous lines) values are shown

TABLE 4 Soil texture data (hydrometer method) for the below-canopy eddy covariance tower at the south-facing slope at the Libby Creek Experimental Watershed on the eastern slope of the Medicine Bow Mountains in south-eastern Wyoming

Depth (cm)	Sand (%)	Silt (%)	Clay (%)	Class
0–10	63	30	7	Sandy loam
10–30	59	33	8	Sandy loam
30–50	86	13	1	Loamy sand
50–100	59	36	5	Sandy loam

again determined using the brute-force method with LAI = LAI_{ref}/CF. Vegetation parameters were again kept constant with time, despite the ongoing beetle outbreak that is causing increased mortality of spruce trees at LCEW. GEOtop was initialized by running the model twice, where the first 3-year simulation period served as a warm-up period for the second 3-year period. The top boundary condition was again determined by incoming precipitation and the canopy and ground surface energy balances. The bottom boundary conditions for soil water flow and soil heat transport were again zero pressure head gradient and zero temperature gradient, respectively.

A contour plot with the objective function values (expressed as dimensionless $RMSE_w$) for all tested CF and n_e combinations is shown in Figure 4c. Contour plots with only weighted sensible heat flux (Figure 4a) and weighted latent heat flux (Figure 4b) in the objective function are also shown. The best overall results were obtained for CF = 0.9 and n_e = 7 (Figure 4c). With LAI = LAI_{ref}/CF, this results in LAI = 3.0/0.9 = 3.3. Similar to before, CF–n_e combinations with CF > 0.6 and n_e > 5 produce relatively similar model errors (Figure 4a–c). Measured and GEOtop modelled canopy air temperature, below-canopy sensible heat flux, canopy air specific humidity, and below-canopy latent heat flux are shown in Figure 5, together with measured and modelled ground surface temperature, snow depth, and profile-average soil temperature. The 30-min to 2-hr measured values and the 30-min modelled values are averaged to either daily or weekly values to facilitate visual comparison for the 3-year simulation period. Below-canopy sensible and latent heat fluxes are defined as positive upwards. Additional model statistics are summarized in Table 6.

Figure 5 shows considerable discrepancies between measured and modelled turbulent fluxes. For example, weekly measured below-canopy sensible heat flux shows a seasonal pattern with mostly positive values in summer and mostly negative values in winter. This seasonal pattern is largely absent in the modelled values. Instead, the modelled H_g values are mostly around zero. The low modelled H_g in summer is due to the underestimation of daytime T_g, in combination with the high optimized value for n_e (=high r_{uc}, see Section 6). The underestimated summer daytime T_g values are not obvious from Figure 5 because of the weekly averaging. Below-canopy latent heat flux is described reasonably well by the model. Snow depth is captured well, but soil temperature is too low during all three winters. Scatter plots comparing the 30-min or 2-hr measured and modelled values (not shown) confirm the large discrepancies between measured and modelled H_g (r^2 = .146). Measured and modelled LE_g agree better (r^2 = .581) but show considerable scatter.

TABLE 5 Estimated soil dry bulk density ρ_b, optimized residual soil water content θ_r, optimized saturated soil water content θ_s, optimized inverse of the air entry soil water pressure head α_{vg}, optimized pore size distribution parameter n, and calculated saturated soil hydraulic conductivity K_s for the below-canopy eddy covariance tower at the south-facing slope at the Libby Creek Experimental Watershed on the eastern slope of the Medicine Bow Mountains in south-eastern Wyoming.

Depth (cm)	ρ_b (g cm^{-3})	θ_r (cm^3 cm^{-3})	θ_s (cm^3 cm^{-3})	α_{vg} (cm^{-1})	n	K_s (cm day^{-1})
0–10	1.0	0.019	0.270	0.150	1.314	39
10–30	0.8	0.010	0.210	0.321	1.239	8
30–50	1.0	0.017	0.284	0.075	1.684	461
50–150	1.2	0.000	0.309	0.142	1.257	80

The mean diurnal variations in H_g and LE_g for different periods and conditions (Figure 6) can be used to analyse the discrepancies in measured and modelled turbulent fluxes. Figure 6 shows that measured daytime H_g values are positive, whereas the modelled daytime H_g values are close to zero. The near-zero modelled H_g fluxes are a result of the underestimation of daytime ground surface temperatures and the high optimized n_e = 7 value, as mentioned earlier. Discrepancies are relatively small for LE_g, although there is a general underestimation of daytime LE_g. Scatter plots with 30-min measured versus 30-min modelled H_g and LE_g values for different periods and conditions (not shown) confirm the model deficiencies (.014 $\leq r^2 \leq$ .561 for H_g; .151 $\leq r^2 \leq$ .643 for LE_g).

5 | BELOW-CANOPY TURBULENT FLUXES: LCEW, NORTH-FACING SLOPE

The GEOtop modelled turbulent fluxes were also verified against data from a second below-canopy eddy covariance tower at the LCEW in south-eastern Wyoming. This second eddy covariance tower is located about 500 m to the west of the first LCEW tower on a

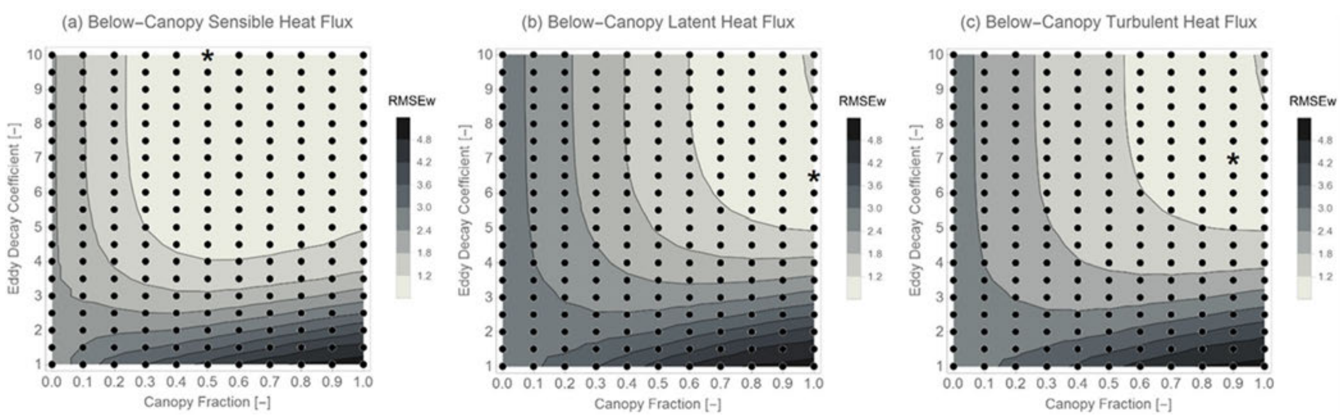

FIGURE 4 Contour plots of model error (expressed as dimensionless weighted root mean square error $RMSE_w$) as a function of canopy fraction and within-canopy eddy decay coefficient for the below-canopy eddy covariance tower (south-facing slope) at the Libby Creek Experimental Watershed in south-eastern Wyoming. The dots represent individual model runs. The stars represent the parameter combination with the lowest model error. Model error was calculated using a weighted objective function containing 30-min below-canopy sensible heat flux (a), latent heat flux (b), and sensible and latent heat fluxes combined (c)

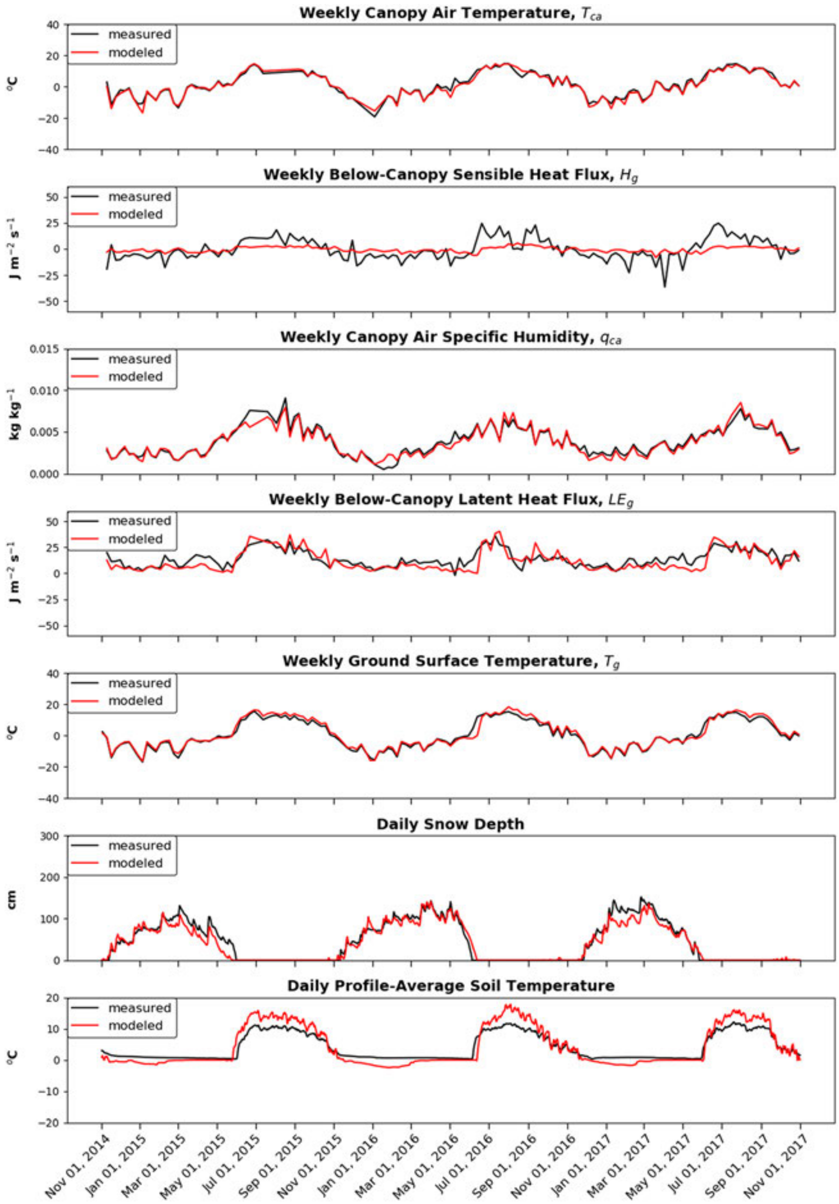

FIGURE 5 Measured and GEOtop modelled canopy air temperature, below-canopy sensible heat flux, canopy air specific humidity, below-canopy latent heat flux, ground surface temperature, snow depth, and profile-average soil temperature for November 2014 to October 2017 for the below-canopy eddy covariance tower (south-facing slope) at the Libby Creek Experimental Watershed in south-eastern Wyoming

TABLE 6 Calculated 30-min to 2-hr interval RMSE, ME, and CRM for the GEOtop model application for the below-canopy eddy covariance tower at the south-facing slope at the Libby Creek Experimental Watershed on the eastern slope of the Medicine Bow Mountains in south-eastern Wyoming

Model component	RMSE	ME	CRM
Canopy air temperature	3.11°C	0.88	0.12
Below-canopy sensible heat flux	36.92 J m^{-2} s^{-1}	0.08	4.47
Canopy air specific humidity	0.00073 kg kg^{-1}	0.85	0.01
Below-canopy latent heat flux	14.61 J m^{-2} s^{-1}	0.57	0.09
Ground surface temperature	3.28°C	0.90	−1.83
Snow depth	12.14 cm	0.93	0.10
Profile-average soil temperature	2.41°C	0.66	−0.07

Abbreviations: CRM, coefficient of residual mass; ME, modelling efficiency; RMSE, root mean square error.

north-facing slope in mixed lodgepole pine, Engelmann spruce, and subalpine fir forest at 2,995 m above mean sea level. The slope (length = 200 m; aspect = 310°; angle = 8°) is generally snow covered from November to June. The simulation period (November 1, 2014, to October 31, 2017), climate data (elevation-corrected 30-min data from GLEES), and instrument setup (IRGASON, SR50, SI-111, and Hydra probes) were the same as for the south-facing LCEW site, with the exception that the IRGASON was installed at 3.1 m instead of 3.5 m above the soil surface.

Soil texture and soil water retention data for the site were limited to a single depth interval (0–15 cm). In GEOtop, a 1.5-m-deep soil profile was assumed consisting of a single layer. The grab sample from the 0- to 15-cm depth was dried, crushed, and sieved (<2-mm diameter) in the laboratory. Soil texture was 39 % sand, 41 % silt, and 20 % clay (class is loam). Gravimetric water retention data were converted to volumetric water retention data using an estimated dry bulk density

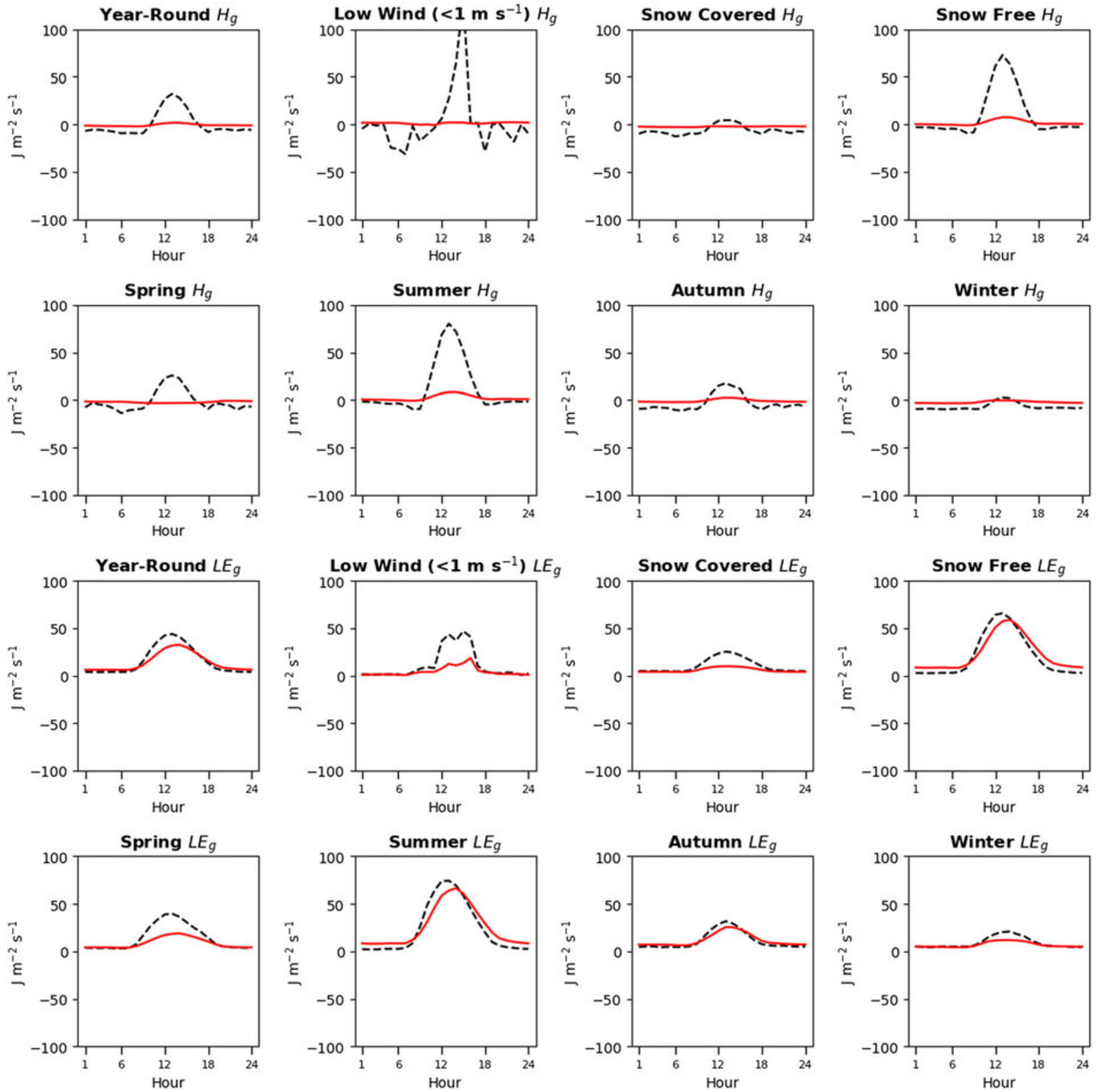

FIGURE 6 Mean diurnal variation of below-canopy sensible heat flux H_g and below-canopy latent heat flux LE_g for different periods and conditions during the November 2014 to October 2017 study period for the below-canopy eddy covariance tower (south-facing slope) at the Libby Creek Experimental Watershed in south-eastern Wyoming. Both measured (black dashed lines) and GEOtop modelled (red continuous lines) values are shown

ρ_b = 1.0 g cm^{-3}. Subsequent curve fitting resulted in van Genuchten water retention parameters of residual soil water content θ_r = 0.000 cm^3 cm^{-3}, saturated soil water content θ_s = 0.386 cm^3 cm^{-3}, inverse of the air entry soil water pressure head α_{vg} = 0.023 cm^{-1}, and pore size distribution parameter n = 1.234. The calculated saturated hydraulic conductivity (Kozeny–Carman equation) was K_s = 9 cm day^{-1}. Vegetation parameters, calibration method, warm-up period, and boundary conditions were the same as for the first LCEW site.

A contour plot with the objective function values (expressed in dimensionless RMSE$_w$) for all tested CF and n_e combinations is shown in Figure 7c. Contour plots with only weighted sensible heat flux (Figure 7a) and weighted latent heat flux (Figure 7b) in the objective function are also shown. The lowest overall model errors were obtained for CF = 0.9 and n_e = 6.5 (Figure 7c), resulting in LAI = 3.3. Measured and GEOtop modelled canopy air temperature, below-canopy sensible heat flux, canopy air specific humidity, and below-canopy latent heat flux are shown in Figure 8, together with measured and modelled ground surface temperature, snow depth, and profile-average soil temperature. The 30-min (T_{ca}, H_g, q_{ca}, and LE_g) and 2-hr (T_g, snow depth, and soil temperature) measured values and the 30-min modelled values are averaged to either daily or weekly values to facilitate visual comparison. As before, the below-canopy sensible and latent heat fluxes are defined as positive upwards. Additional model statistics are summarized in Table 7.

The comparison between measured and modelled below-canopy turbulent fluxes shows similar discrepancies as for the south-facing

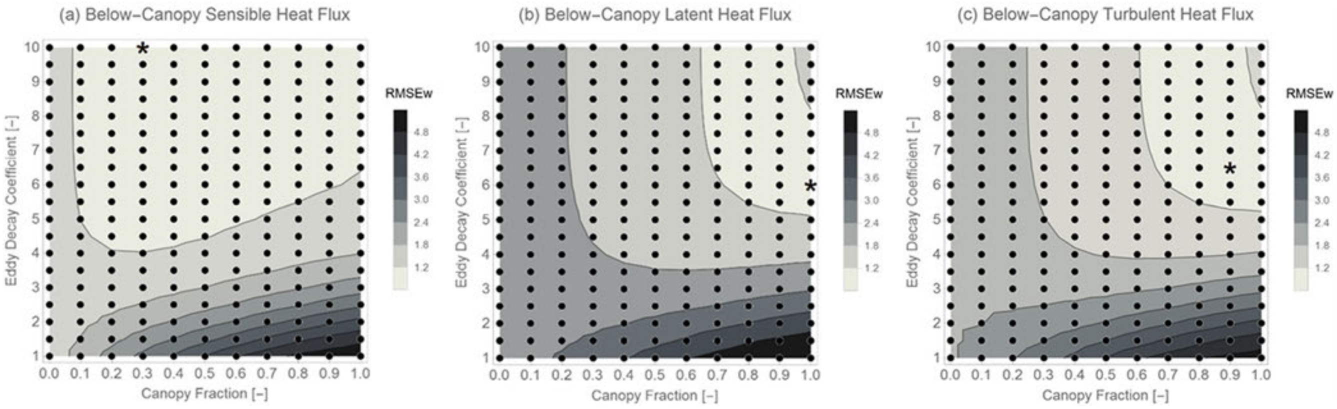

FIGURE 7 Contour plots of model error (expressed as dimensionless weighted root mean square error $RMSE_w$) as a function of canopy fraction and within-canopy eddy decay coefficient for the below-canopy eddy covariance tower (north-facing slope) at the Libby Creek Experimental Watershed in south-eastern Wyoming. The dots represent individual model runs. The stars represent the parameter combination with the lowest model error. Model error was calculated using a weighted objective function containing 30-min below-canopy sensible heat flux (a), latent heat flux (b), and sensible and latent heat fluxes combined (c)

LCEW site. Weekly measured below-canopy sensible heat flux again shows a clear seasonal pattern with mostly positive values in summer and mostly negative values in winter. In contrast, weekly modelled H_g values are close to zero or negative. Weekly below-canopy latent heat flux is described reasonably well by the model. Measured snow on the north-facing slope (Figure 8) is considerably deeper than is measured snow on the south-facing slope (Figure 5). The modelled snow depths only partially reflect this, with snow depth being underestimated for all three years in Figure 8. Modelled soil temperatures are again too low in early-winter. Scatter plots comparing 30-min or 2-hr measured and modelled values (not shown) confirm the large discrepancies between measured and modelled H_g (r^2 = .031). Measured and modelled LE_g again agree better (r^2 = .445).

The mean diurnal variations in H_g and LE_g (Figure 9) confirm earlier observations for the south-facing slope that measured daytime H_g values are positive whereas modelled daytime H_g values are mostly around zero. Results for LE_g also confirm earlier observations with modelled daytime values being generally too low. Scatter plots with 30-min measured versus 30-min modelled H_g and LE_g values for different periods and conditions (not shown) confirm the serious model deficiencies for H_g (.000 $\leq r^2 \leq$ .288) and the better results for LE_g (.113 $\leq r^2 \leq$ .546).

6 | DISCUSSION

In this study, GEOtop modelled above- and below-canopy turbulent fluxes in snow-dominated mountain forest are compared against eddy covariance measurements. The model is informed using field-observed vegetation parameters and laboratory-measured gravimetric soil water retention. Model calibration is limited to finding the optimum combination of canopy fraction and the dimensionless eddy decay coefficient. Volumetric soil water retention is calculated from measured gravimetric soil water retention. Dry bulk densities for the stony soils are estimated but not optimized.

Above-canopy sensible heat flux H is captured reasonably well (r^2 = .851) with relatively high upward flux during daytime and relatively low downward flux during night-time, as expected. Above-canopy latent heat flux LE is less well predicted (r^2 = .426). Interestingly, mean diurnal trends in LE are captured reasonably well (Figure 3), suggesting that the overall moisture exchange between the canopy air and the atmosphere is captured well by the model. The poor model prediction of individual (30-min) LE values may be due to imperfections in the modelled bio-physical relationships (i.e., the interrelationships between soil, plant, and atmosphere) or point to knowledge gaps in our understanding of turbulent moisture exchange. Similar results are reported by Mahat et al. (2013) who applied the Utah Energy Balance model to above-canopy eddy covariance data from Niwot Ridge, Colorado (mixed coniferous forest), and found average r^2 = .67 for H and average r^2 = .24 for LE for nine winter periods. As in our study, individual LE values showed high variation, whereas mean diurnal trends in LE were reasonably quantified.

Below-canopy sensible heat flux is being underestimated during daytime and overestimated during night-time (Figures 6 and 9). In addition, below-canopy latent heat flux is being underestimated during daytime. The above discrepancies are attributed to the high (optimized) n_e values of 6.5 (Figure 7) and 7.0 (Figure 4). High n_e results in high r_{uc} (Equation 9) and low below-canopy turbulent exchange. Lower values of n_e (lower r_{uc}) would have resulted in unrealistically large negative (downward) daytime H_g and large positive (upward) LE_g, especially during winter when the soil is snow covered (results not shown). The large negative daytime H_g for low n_e is the result of not enough solar radiation reaching the ground surface, resulting in too low T_g and H_g having the wrong sign (negative instead of positive). The large positive LE_g for low n_e during winter can be understood by considering that the water vapour pressure in snow is always at saturation, providing an unlimited supply of water to the atmosphere.

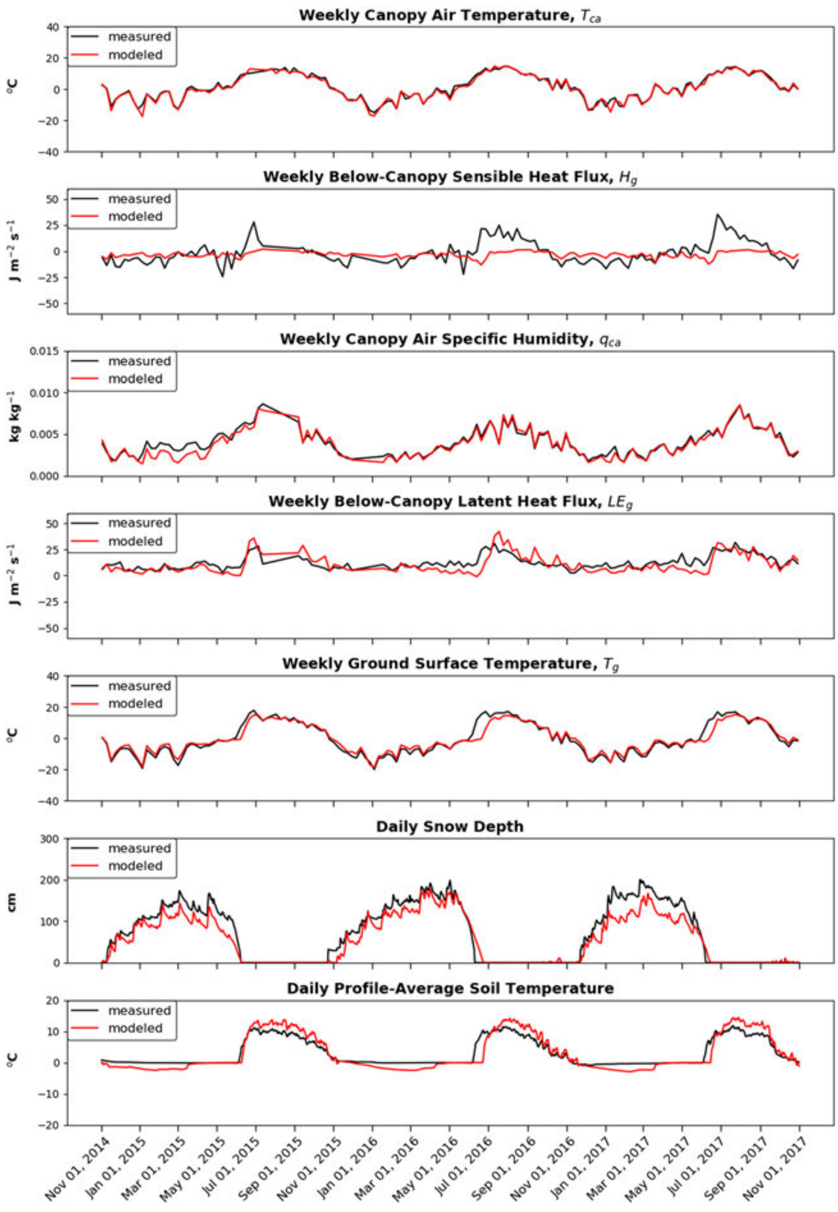

FIGURE 8 Measured and GEOtop modelled canopy air temperature, below-canopy sensible heat flux, canopy air specific humidity, below-canopy latent heat flux, ground surface temperature, snow depth, and profile-average soil temperature for November 2014 to October 2017 for the below-canopy eddy covariance tower (north-facing slope) at the Libby Creek Experimental Watershed in south-eastern Wyoming

TABLE 7 Calculated 30-min to 2-hr interval RMSE, ME, and CRM for the GEOtop model application for the below-canopy eddy covariance tower at the north-facing slope at the Libby Creek Experimental Watershed on the eastern slope of the Medicine Bow Mountains in south-eastern Wyoming

Model component	RMSE	ME	CRM
Canopy air temperature	3.31°C	0.87	0.17
Below-canopy sensible heat flux	37.27 J m^{-2} s^{-1}	0.03	−2.56
Canopy air specific humidity	0.00074 kg kg^{-1}	0.84	0.03
Below-canopy latent heat flux	15.18 J m^{-2} s^{-1}	0.41	0.07
Ground surface temperature	6.46°C	0.75	0.23
Snow depth	23.06 cm	0.88	0.20
Profile-average soil temperature	2.10°C	0.75	0.04

Abbreviations: CRM, coefficient of residual mass; ME, modelling efficiency; RMSE, root mean square error.

Modelled H_g can be improved by selecting a lower value for CF of 0.3–0.5 as suggested by Figures 4a and 7a. With low CF, more solar radiation reaches the ground surface, resulting in higher T_g and H_g having a positive sign. However, a lower value of CF also results in overestimated (positive) LE_g during periods with snow cover or wet soils (results not shown). Summer LE_g is not affected by lower CF values because soils are generally dry and the water vapour supply to the atmosphere is limited.

The underestimation of daytime T_g, and the associated discrepancies in H_g with CF = 0.9, are not restricted to winter periods but happen year-round. As an example, Figure 10 shows measured and modelled T_{ca}, T_g, $T_g - T_{ca}$, and H_g for an 11-day period in July at the LCEW, south-facing slope site. On cloudless days especially (from the third day onwards), the figure shows that daytime T_g is underestimated whereas night-time T_{ca} and T_g are overestimated. This suggests that not enough solar radiation reaches the soil surface

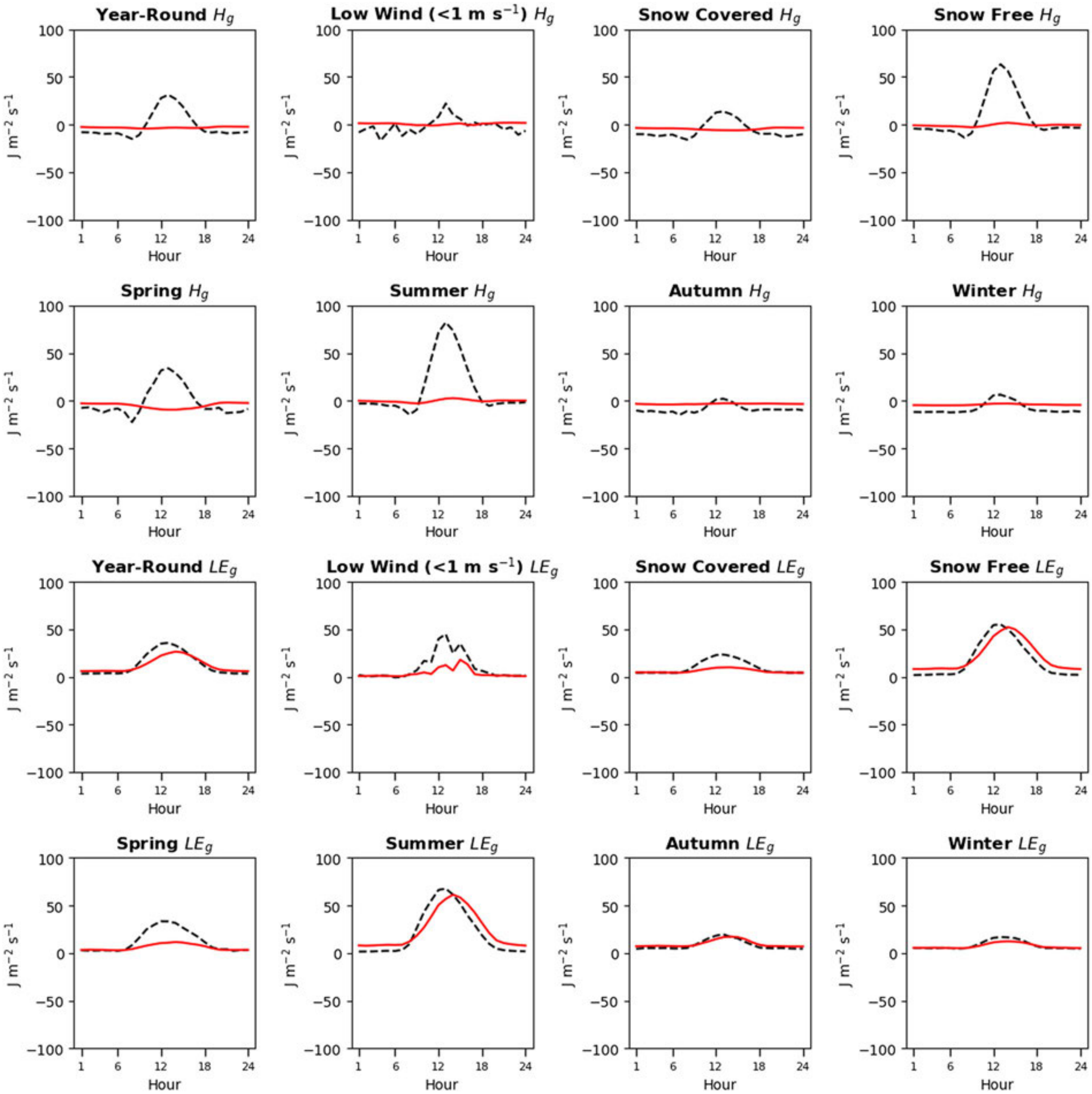

FIGURE 9 Mean diurnal variation of below-canopy sensible heat flux H_g and below-canopy latent heat flux LE_g for different periods and conditions during the November 2014 to October 2017 study period for the below-canopy eddy covariance tower (north-facing slope) at the Libby Creek Experimental Watershed in south-eastern Wyoming. Both measured (black dashed lines) and GEOtop modelled (red continuous lines) values are shown

during the day, whereas insufficient long wave radiation is emitted towards the atmosphere at night.

The brute-force calibration identifies CF = 0.9 and n_e = 6.5–7.0 as the best compromise for describing the below-canopy turbulent fluxes. The high n_e limits the underestimation of H_g and the overestimation of LE_g by setting r_{uc} to a high value. In addition, the high CF value further limits the overestimation of LE_g at the expense of H_g, which would have benefitted from a lower CF value. The optimum eddy decay coefficient $6.5 \le n_e \le 7$ is relatively high than that of previous studies (e.g., Brutsaert, 1982).

Snow depth ($.897 \le r^2 \le .951$), snow water equivalent (r^2 = .839), ground heat flux (r^2 = .326), and soil temperature ($.699 \le r^2 \le .954$) are modelled with variable success in this study. Our study sites in south-eastern Wyoming experience high winds during most of the year, which not only complicates the measurement of precipitation due to snowfall but also results in significant lateral snow redistribution. Given the associated uncertainties in model input (winter precipitation) and measured data (snow depth and snow water equivalent), we find GEOtop's performance satisfactory using only default snow parameters (no calibration). For GLEES, this results in delayed melt-

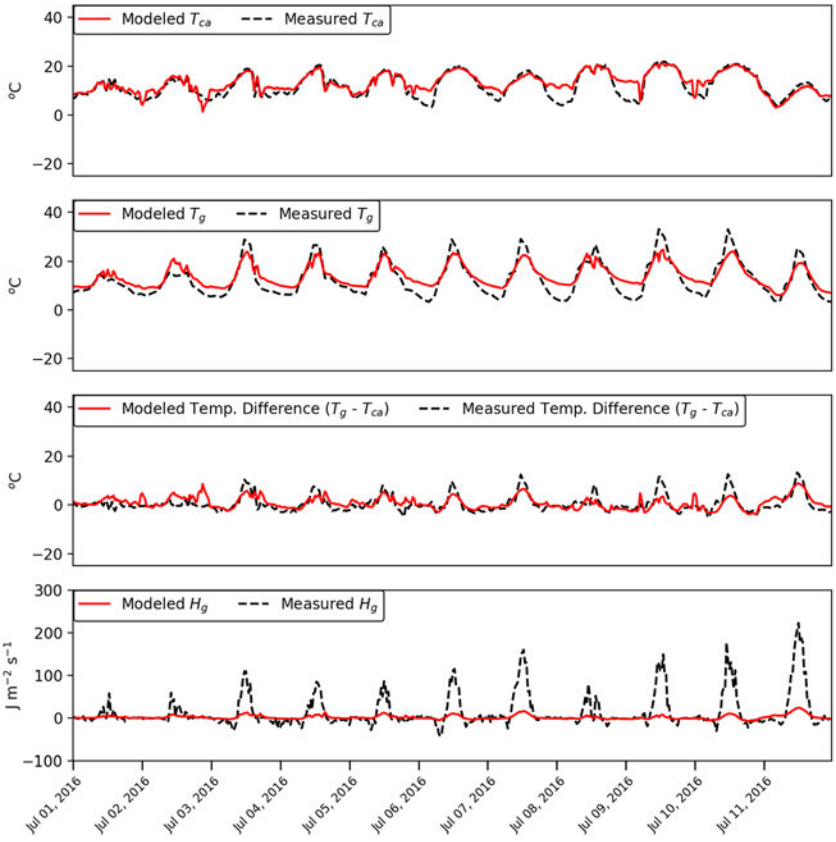

FIGURE 10 Measured and GEOtop modelled canopy air temperature T_{ca}, ground surface temperature T_g, T_g–T_{ca}, and below-canopy sensible heat flux H_g for July 1, 2016, to July 11, 2016, for the below-canopy eddy covariance tower (south-facing slope) at the Libby Creek Experimental Watershed in south-eastern Wyoming

off for most years, whereas for LCEW, this results in underestimated snow depths for most years (Figures 2, 5, and 8). The opposing model performance with regard to snow (too much snow at GLEES; not enough snow at LCEW) suggests that altering snow parameters alone is unlikely to improve model results.

The trade-offs between the description of leaf area index, canopy fraction, and eddy decay coefficient, and their effect on the ground surface energy balance in forests warrant further study. Having canopy fractions of 0.3–0.7 seem to result in more realistic ground surface temperatures and more realistic below-canopy sensible heat fluxes. However, in GEOtop, this also results in too high below-canopy latent heat fluxes. Another concern is that, with current models, having CF < 1 results in having different wind functions for the vegetated and bare ground fractions at the plot scale, where there should be only one.

7 | CONCLUSION

This study examined the effectiveness of the GEOtop model in calculating above- and below-canopy turbulent fluxes in snow-dominated mountain forest. Above-canopy sensible heat flux was predicted reasonably well (r^2 = .851), whereas above-canopy latent heat flux was less well predicted (r^2 = .426). Mean diurnal trends were well predicted, for both sensible and latent heat fluxes. For the above-canopy latent heat flux, this indicates that errors in 30-min values offset each other when fluxes are aggregated over time. Below-canopy turbulent fluxes were predicted with variable success with r^2 = .031–.146 for sensible heat flux and r^2 = .445–.581 for latent heat flux. Modelled below-canopy sensible heat flux was mostly zero or directed downwards, even during summer when measured daytime sensible heat fluxes were clearly upwards, as would be expected. This discrepancy was attributed to not enough solar radiation reaching the ground surface in the model, despite allowing for canopy fractions < 1, and resulting in too low surface temperatures. A relatively high dimensionless eddy decay coefficient of 6.5–7.0 was used in this study to describe the within-canopy wind profile. The high decay coefficient (=high undercanopy resistance) was needed to limit below-canopy turbulent flux over snow especially to reasonable values.

ACKNOWLEDGMENTS

This work was supported by the National Science Foundation funded Wyoming Center for Environmental Hydrology and Geophysics under Grant EPS-1208909.

DATA AVAILABILITY STATEMENT

The data that support the findings of this study are available from the corresponding author upon reasonable request.

ORCID

Thijs J. Kelleners https://orcid.org/0000-0002-4004-1267
John M. Frank https://orcid.org/0000-0001-6543-0333
William J. Massman https://orcid.org/0000-0002-5628-6437

REFERENCES

Bales, R. C., Molotch, N. P., Painter, T. H., Dettinger, M. D., Rice, R., & Dozier, J. (2006). Mountain hydrology of the western United States. *Water Resources Research*, *42*, W08432. https://doi.org/10.1029/2005WR004387

Bear, J. (1972). *Dynamics of fluids in porous media* (p. 764). New York, NY: American Elsevier Publishing Company, Inc.

Bertoldi, G., Notarnicola, C., Leitinger, G., Endrizzi, S., Zebisch, M., Della Chisa, S., & Tappeiner, U. (2010). Topographical and ecohydrological controls on land surface temperature in an Alpine catchment. *Journal of Ecohydrology*, *3*, 189–204.

Best, M. J. (1998). A model to predict surface temperatures. *Boundary-Layer Meteorology*, *88*, 279–306. https://doi.org/10.1023/A:1001151927113

Brutsaert, W. (1982). *Evaporation into the atmosphere: Theory, history and applications. D. Reidel Publishing Company* (p. 299). Netherlands: Dordrecht. https://doi.org/10.1007/978-94-017-1497-6

Chen, F., Barlage, M., Tewari, M., Rasmussen, R., Jin, J., Lettenmaier, D., … Yang, Z.-L. (2014). Modeling seasonal snowpack evolution in the complex terrain and forested Colorado Headwaters region: A model intercomparison study. *Journal of Geophysical Research – Atmospheres*, *119*, 13,795–13,819. https://doi.org/10.1002/2014JD022167

Clausnitzer, V. and Hopmans, J.W. 1995. Non-linear parameter estimation: LM_OPT. General-purpose optimization code based on the Levenberg–Marquardt algorithm. Land, Air, and Water Resources Paper No. 100032, University of California, Davis, CA.

Dane, J. H., & Hopmans, J. W. (2002a). Pressure plate extractor. In J. H. Dane, & G. C. Topp (Eds.), *Methods of soil analysis, Part 4: Physical methods* (pp. 688–690). Madison, WI: Soil Science Society of America.

Dane, J. H., & Hopmans, J. W. (2002b). Hanging water column. In J. H. Dane, & G. C. Topp (Eds.), *Methods of soil analysis, Part 4: Physical methods* (pp. 680–683). Madison, WI: Soil Science Society of America.

Della Chiesa, S., Bertoldi, G., Niedrist, G., Obojes, N., Endrizzi, S., Albertson, J. D., … Tappeiner, U. (2014). Modelling changes in grassland hydrological cycling along an elevational gradient in the Alps. *Ecohydrology*, *7*(6), 1453–1473. https://doi.org/10.1002/eco.1471

Dolman, A. J. (1993). A multiple-source land surface energy balance model for use in general circulation models. *Agricultural and Forest Meteorology*, *65*, 21–45. https://doi.org/10.1016/0168-1923(93)90036-H

Endrizzi, S., Gruber, S., Dall Amico, M., & Rigon, R. (2014). GEOtop 2.0: Simulating the combined energy and water balance at and below the land surface accounting for soil freezing, snow cover and terrain effects. *Geoscientific Model Development Discussion*, *7*, 2831–2857. https://doi.org/10.5194/gmd-7-2831-2014

Endrizzi, S., & Marsh, P. (2010). Observations and modeling of turbulent fluxes during melt at the shrub-tundra transition zone 1: Point scale variations. *Hydrology Research*, *41*(6), 471–491. https://doi.org/10.2166/nh.2010.149

Flerchinger, G. N., Reba, M. L., & Marks, D. (2012). Measurement of surface energy fluxes from two rangeland sites and comparison with a multilayer canopy model. *Journal of Hydrometeorology*, *13*, 1038–1051. https://doi.org/10.1175/JHM-D-11-093.1

Frank, J. M., Massman, W. J., Ewers, B. E., Huckaby, L. S., & Negrón, J. F. (2014). Ecosystem CO_2/H_2O fluxes are explained by hydraulically limited gas exchange during tree mortality from spruce bark beetles. *Journal of Geophysical Research. Biogeosciences*, *119*, 1195–1215. https://doi.org/10.1002/2013JG002597

Fullhart, A. T., Kelleners, T. J., Chandler, D. G., McNamara, J. P., & Seyfried, M. S. (2018). Water flow modeling with dry bulk density optimization to determine hydraulic properties in mountain soils. *Soil Science Society of America Journal*, *82*, 31–44. https://doi.org/10.2136/sssaj2017.06.0196

Fullhart, A. T., Kelleners, T. J., Chandler, D. G., McNamara, J. P., & Seyfried, M. S. (in press). Modeling snowmelt-driven streamflow from two small Rocky Mountain catchments using the GEOtop model. *Hydrological Processes*.

Hingerl, L., Kunstmann, H., Wagner, S., Mauder, M., Bliefernicht, J., & Rigon, R. (2016). Spatio-temporal variability of water and energy fluxes—A case study for a mesoscale catchment in pre-alpine environment. *Hydrological Processes*, *30*(21), 3804–3823. https://doi.org/10.1002/hyp.10893

Kelleners, T. J., Koonce, J., Shillito, R., Dijkema, J., Berli, M., Young, M. H., … Massman, W. J. (2016). Numerical modeling of coupled water flow and heat transport in soil and snow. *Soil Science Society of America Journal*, *80*, 247–263. https://doi.org/10.2136/sssaj2015.07.0279

Kochendorfer, J. P., & Ramirez, J. A. (2010). Ecohydrologic controls on vegetation density and evapotranspiration partitioning across the climatic gradients of the central United States. *Hydrology and Earth System Sciences*, *14*, 2121–2139. https://doi.org/10.5194/hess-14-2121-2010

Lee, T. J., & Pielke, R. A. (1992). Estimating the soil surface specific humidity. *Journal of Applied Meteorology*, *31*, 480–484. https://doi.org/10.1175/1520-0450(1992)031<0480:ETSSSH>2.0.CO;2

Liston, G. E., & Elder, K. (2006). A meteorological distribution system for high-resolution terrestrial modeling (MicroMet). *Journal of Hydrometeorology*, *7*, 217–234. https://doi.org/10.1175/JHM486.1

Loague, K., & Green, R. E. (1991). Statistical and graphical methods for evaluating solute transport models: Overview and application. *Journal of Contaminant Hydrology*, *7*, 51–73. https://doi.org/10.1016/0169-7722(91)90038-3

Mahat, V., Tarboton, D. G., & Molotch, N. P. (2013). Testing above- and below-canopy representations of turbulent fluxes in an energy balance snowmelt model. *Water Resources Research*, *49*, 1107–1122. https://doi.org/10.1002/wrcr.20073

Massman, W. J., & Lee, X. (2002). Eddy covariance flux corrections and uncertainties in long-term studies of carbon and energy exchanges. *Agricultural and Forest Meteorology*, *113*, 121–144. https://doi.org/10.1016/S0168-1923(02)00105-3

Mauder, M., Genzel, S., Fu, J., Kiese, R., Soltani, M., Steinbrecher, R., … Kunstmann, H. (2018). Evaluation of energy balance closure adjustment methods by independent evapotranspiration estimates from lysimeters and hydrological simulations. *Hydrological Processes*, *32*, 39–50. https://doi.org/10.1002/hyp.11397

Moene, A. F., & van Dam, J. C. (2014). *Transport in the atmosphere–vegetation–soil continuum* (Vol. 446). New York, NY: Cambridge University Press.

Monin, A.S. and Obukhov A.M.. 1954. Basic laws of turbulent mixing in the surface layer of the atmosphere. Tr Akad Nauk SSSR Geophiz Inst 24:163-187.

Monson, R., & Baldocchi, D. (2014). *Terrestrial biosphere–atmosphere fluxes* (Vol. 487). New York, NY: Cambridge University Press. https://doi.org/10.1017/CBO9781139629218

Mualem, Y. (1976). A new model for predicting the hydraulic conductivity of unsaturated porous media. *Water Resources Research*, *12*, 513–522. https://doi.org/10.1029/WR012i003p00513

Pleasants, M. S., Kelleners, T. J., & Ohara, N. (2017). Analysis of snowpack dynamics during the spring melt season for a sub-alpine site using point measurements and numerical modeling. *Hydrological Processes*, *31*, 4568–4585. https://doi.org/10.1002/hyp.11379

Reed, D. E., Frank, J. M., Ewers, B. E., & Desai, A. R. (2017). Time dependency of eddy covariance site energy balance. *Agricultural and Forest Meteorology*, *249*, 467–478.

Rigon, R., Bertoldi, G., & Over, T. M. (2006). GEOtop: A distributed hydrological model with coupled water and energy budgets. *Journal of Hydrometeorology*, *7*, 371–388. https://doi.org/10.1175/JHM497.1

Russo, D. (1983). Leaching characteristics of a stony desert soil. *Soil Science Society of America Journal*, *47*, 431–438. https://doi.org/10.2136/sssaj1983.03615995004700030008x

Speckman, H. N., Frank, J. M., Bradford, J. B., Miles, B. L., Massman, W. J., Parton, W. J., & Ryan, M. G. (2015). Forest ecosystem respiration estimated from eddy covariance and chamber measurements under high turbulence and substantial tree mortality from bark beetles. *Global Change Biology*, *21*, 708–721. https://doi.org/10.1111/gcb.12731

van Genuchten, M. T. (1980). A closed-form equation for predicting the hydraulic conductivity of unsaturated soils. *Soil Science Society of America Journal*, *44*, 892–898. https://doi.org/10.2136/sssaj1980.03615995004400050002x

Ye, Z., & Pielke, R. A. (1993). Atmospheric parameterization of evaporation from non-plant-covered surfaces. *Journal of Applied Meteorology*, *32*, 1248–1258. https://doi.org/10.1175/1520-0450(1993)032<1248:APOEFN>2.0.CO;2

How to cite this article: Fullhart AT, Kelleners TJ, Speckman HN, et al. Measured and modelled above- and below-canopy turbulent fluxes for a snow-dominated mountain forest using GEOtop. *Hydrological Processes*. 2019;33:2464–2480. https://doi.org/10.1002/hyp.13487